Single-Nanocrystal Photoluminescence Spectroscopy Studies of Plasmon–Multiexciton Interactions at Low Temperature

DATASET · MARCH 2013

1 AUTHOR:

Ping Xu
Harbin Institute of Technology
101 PUBLICATIONS **2,932** CITATIONS

SEE PROFILE

THE JOURNAL OF PHYSICAL CHEMISTRY Letters

Letter

pubs.acs.org/JPCL

Single-Nanocrystal Photoluminescence Spectroscopy Studies of Plasmon−Multiexciton Interactions at Low Temperature

Young-Shin Park,[†,‡,§] Yagnaseni Ghosh,[‡] Ping Xu,[†] Nathan H. Mack,[†] Hsing-Lin Wang,[†] Jennifer A. Hollingsworth,[‡] and Han Htoon*[,†,‡]

[†]Chemistry Division and [‡]Center for Integrated Nanotechnologies, Materials Physics & Applications Division, Los Alamos National Laboratory, Los Alamos, New Mexico 87545, United States

Supporting Information

ABSTRACT: Using thick-shell or "giant" CdSe/CdS nanocrystal quantum dots (g-NQDs), characterized by strongly suppressed Auger recombination, we studied the influence of plasmonic interactions on multiexciton emission. Specifically, we assessed the separate effects of plasmonic absorption and plasmonic emission enhancement by a systematic analysis of the pump fluence dependence of low-temperature photoluminescence (low-T PL) derived from individual CdSe/CdS g-NQDs deposited on nanoroughened silver films. Our study reveals that (1) the multiexciton (MX) emissions in g-NQD coupled to silver films were enhanced not only through the creation of more excitons via enhancement of absorption but also through the direct modification of the competition between the radiative and nonradiative recombination processes of MXs; (2) strong enhancement in absorption is not necessary for strong multiexciton emission; and (3) the emission of MXs can become stronger with the increase of multiexciton order. We also exploited the strong enhancement of MX emission to perform second-order photon correlation and cross-correlation experiments using very low pump fluences and observed a strong photon bunching that decays with increasing pump fluence.

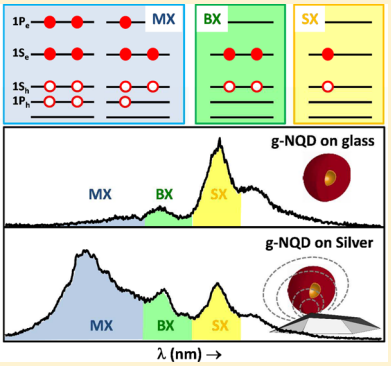

SECTION: Spectroscopy, Photochemistry, and Excited States

Efficient radiative recombination of multiexciton (MX) complexes in epitaxially grown semiconductor quantum dots has enabled the development of electrically pumped low-threshold lasers[1,2] and entangled photon pair sources.[3−5] In contrast, conventional colloidal nanocrystal quantum dots (NQDs) cannot be utilized efficiently in such applications because the radiative emission of their MXs is strongly quenched by a very efficient nonradiative Auger recombination (AR) process.[6] Recently, however, new types of heterostructured NQDs that afford emission from MX states[7−10] have been developed. One such AR-suppressed NQD is the so-called "giant" NQD (g-NQD), which is characterized by a highly crystalline thick shell and additional characteristics such as suppressed blinking and photobleaching.[11−14] Even in this case where strong AR suppression has been shown,[15] the biexciton (BX) quantum yield (QY) remains lower than that of the single-exciton (SX) states.[16] Importantly, due to the increase in available recombination channels, MX AR decay rates ($k_{A,mX}$) scale with their order m as $k_{A,mX} = m^2(m-1)k_{A,2X}/4$, while MX radiative recombination rates ($k_{R,mX}$) scale more slowly as $k_{R,mX} = m^2k_{R,X}$.[17] As a result, MX emission efficiencies (Q_{mX}) become successively weaker as m increases and, therefore, become inaccessible for light-emission applications. Thus, further suppression of AR or *enhancement* of MX emission is needed to realize universally bright emission from higher-order MX states.

To achieve the latter (MX enhancement), plasmonic interactions can be used as an "extrinsic" approach in tuning MX emission efficiencies. Plasmonic (nanometallic) structures are characterized by strong gradients in the local electromagnetic field that can not only modify the radiative recombination rate of MXs[18] but also change MX "symmetry", opening normally forbidden MX transitions.[19,20] Therefore, in addition to simple enhancement of emission efficiencies, plasmon−MX interactions may be able to break or revert the successive weakening of MX emission efficiencies. To date, however, studies of NQD−metal nanostructure (MN) coupled systems have been limited to plasmon−SX interactions. Although these studies revealed valuable information pertaining to SX photoluminescence (PL) enhancement and even modification of blinking behavior and PL decay dynamics,[21−23] MX−plasmon interactions remain comparatively unexplored. Furthermore, to our best knowledge, a low-temperature (T) single-nanostructure optical spectroscopy study, which is very powerful in distinguishing the emission of MXs in the spectral domain,[7,8,24,25] has not been applied to NQD−MN coupled systems.

We performed low-T PL, time-resolved PL (TRPL), and second-order photon correlation/cross-correlation spectrosco-

Received: March 4, 2013
Accepted: April 10, 2013

   dx.doi.org/10.1021/jz400479t | J. Phys. Chem. Lett. 2013, 4, 1465−1470

py studies on individual CdSe/CdS g-NQDs sparsely dispersed on nanoroughed silver films composed of an assembly of silver nanoflakes (see ref 26 and section SI 1, Supporting Information) Our SX-BX second-order photon cross-correlation and MX second-order photon auto-correlation experiments revealed a very strong photon bunching and a decrease in the degree of photon bunching (i.e., the area ratio between center and side peaks of second-order photon correlation function) as the laser pump fluence is increased. Both of these features are characteristic of the quantum cascade recombination of MX and were impossible to observe in referenced g-NQDs due to successive weakening of Q_{mX}s. Furthermore, we decoupled the plasmonic enhancement between absorption and emission processes and directly compared the MX emission spectra taken at similar exciton occupancy from g-NQDs spread on rough metal surfaces with those of referenced g-NQDs deposited on quartz. This comparison clearly reveals that the MX emission of g-NQDs on a rough silver film can emerge at the exciton occupancy at nearly 1 order of magnitude lower than what is usually observed in reference g-NQDs. In some g-NQDs on silver films, MX emission rises with exciton occupancy without showing any saturation and completely dominates the SX emission at the highest exciton occupancies.

The g-NQDs utilized in this experiment are characterized with a 3 nm diameter CdSe core and a 16 monolayer (ML) thick CdS shell.[11,12] Our prior studies revealed that these g-NQDs are completely free of fluorescence intermittency (blinking)[11,12,27] and can exhibit an average Q_{BX} of up to 20% due to the strong suppression of nonradiative AR.[16] Our recent low-T PL study also demonstrated that PL peaks of MXs can also be observed using both pulse and steady-state excitations.[7] We dispersed these NQDs (density < 0.1 μm^{-2}) onto crystalline quartz substrates (for reference) and rough metal films. The samples were mounted in a continuous flow liquid He cryostat cooled down to 4 K and excited with 405 nm, 40 ps laser pulses. A standard micro-PL setup is used to perform PL, TRPL, and second-order photon correlation spectroscopies.

Figure 1a displays the evolution of the PL spectra of a single g-NQD on silver films as a function of pump fluence. At the lowest pump fluence, the PL spectrum shows the emission of SX (m = 1) and its phonon replica. The BX (m = 2) peak (590 nm) and higher-order MX ($m \geq 3$) band (560−585 nm) emerge when the pump fluence is increased beyond ~0.10 $\mu J/cm^2$. Similar pump-dependent evolution was observed on all individual g-NQDs coupled to silver films. However, the shape, energy separation, and relative strength of BX and higher-order MX bands vary widely from one g-NQD to another. The PL decay curve acquired at the lowest pump fluence (0.014 $\mu J/cm^2$) (Figure 1b) yields 1.8 ns for the lifetime of the SX state (τ_{SX}) for this g-NQD. Similar studies on ~65 referenced g-NQDs and g-NQDs deposited on the silver film reveal that while τ_{SX}'s of reference g-NQDs are distributed widely within the 3.6−15.9 ns range, those of g-NQDs on silver films appear to be shorter than 5.9 ns (see Figure S2(a), Supporting Information).

In order to prove the quantum cascade nature of MX and investigate the efficiency and dynamics of their recombination, we performed second-order photon correlation/cross-correlation spectroscopy studies. Figure 1c displays second-order photon correlation functions of spectrally integrated PL emission (upper panel) and that of spectrally isolated the SX emission band (lower panel) taken at 0.014 $\mu J/cm^2$. The $g^{(2)}$

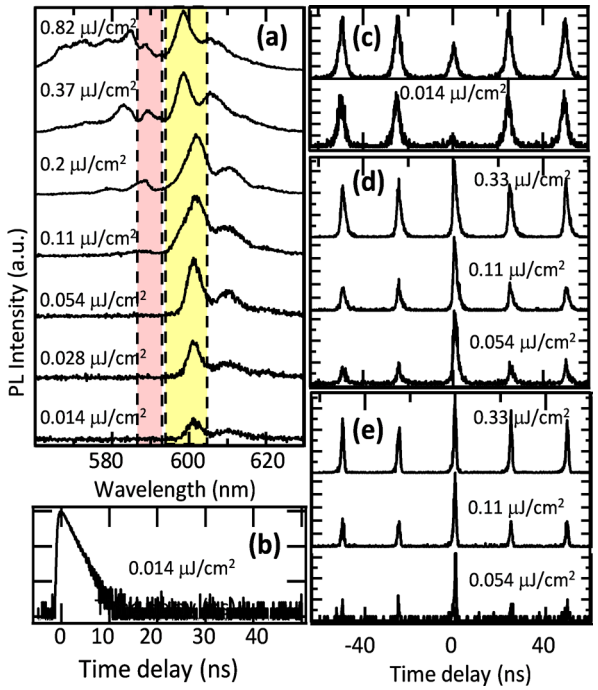

Figure 1. (a) Low-temperature PL spectra of an individual g-NQD displayed in order of increasing pump fluence. (b) PL decay measured at a pump fluence of 0.014 $\mu J/cm^2$. (c) The $g^{(2)}$ functions of spectrally integrated PL providing a measure of BX to SX QY ratio (upper) and that of the SX line showing near-complete photon antibunching. BX−SX cross-correlation function (d) and auto-correlation function of higher-order MXs (e) measured as a function of increasing pump fluences. Pump fluences for $g^{(2)}$ traces in (c−e) are listed on top of each trace.

trace of SX shows nearly complete antibunching as expected for single g-NQDs. On the other hand, the $g^{(2)}$ of spectrally integrated PL shows an incomplete antibunching with a center to side peak area ratio of 0.5, despite the fact that the PL spectrum collected at the same pump power (the lowest row of Figure 1a) shows no sign of MX emission. This happens because the spectrally integrated $g^{(2)}$ experiment is designed to selectively measure the BX → SX quantum cascade process. Prior studies further revealed that this ratio remains constant at very low pump power and provides a measure of the ratio of the QYs of BX and SX states ($R = Q_{BX}/Q_{SX}$)[16,28] (see section SI 2, Supporting Information). The measured R values for reference g-NQDs vary from 0 to 0.64 with an average of (0.35 ± 0.15) and from 0.3 to 1.0 with an average of (0.66 ± 0.21) for g-NQDs on silver film (Figure S2(b), Supporting Information). The g-NQDs' coupling to the silver film leads to an enhancement factor of 1.9 in averaged R values. This enhancement and the wide distribution of R values were also observed at room temperature and are discussed in detail in Supporting Information section SI 3 and ref 29.

Very strong photon bunching and asymmetric peaks are observed in the SX−BX cross-correlation function $g^{(2)}_{SX,BX}$ (Figure 1d), (SX and BX bands are indicated in Figure 1a). The asymmetric peaks of the $g^{(2)}_{SX,BX}$ function reflect the ordered nature of the BX → SX quantum cascade process.[30−33] A similar asymmetric $g^{(2)}_{SX,BX}$ function has been observed in a room-temperature exciton−triexciton cross-correlation experiment on CdSe/ZnS NQDs.[34] However, due to the very weak nature of MX emission, to the best of our knowledge, the pump dependence of $g^{(2)}_{SX,BX}$ has not been studied systematically in any

dx.doi.org/10.1021/jz400479t | J. Phys. Chem. Lett. 2013, 4, 1465−1470

type of colloidal NQDs until this present work. Strong MX emission of our g-NQD on silver films allowed us to perform this experiment. Our data show that the degree of photon bunching increases with the decrease of the pump power, reaching R values of 3.9 at the lowest pump fluence (bottom $g^{(2)}$ of Figure 1d). It can be shown readily (see section SI 2, Supporting Information) that the area of the center peak of $g^{(2)}_{SX,BX}$ in the low-fluence limit scales with the square of the pump power as it is defined by the probability of exciting BX and that of detecting two photons emitted from the BX−SX quantum cascade process on the two APDs used in a Hanbuary, Brown, and Twiss configuration. Similarly, the area of the side peak can be shown to scale with the cube of the pump power as it is defined by the probability of exciting and detecting BX and SX in two successive pulse excitations. As a result, their ratio (the degree of photon bunching) scales inversely with the pump power.

A similar strong photon bunching (R > 5.5) and inverse scaling with pump power was also observed when we performed the photon correlation experiment on the MX band ($g^{(2)}_{MX}$ with $m \geq 2$) (560−585 nm) (Figure 1e). In this case, the inverse pump fluence dependence on the degree of the photon bunching results from the fact that while the area of the center peak is mainly defined by the probability of exciting triexcitons (TXs) and therefore scale with the cube of the pump fluence, the area of the side peak is defined by the probability of exciting BXs in two successive pulse excitations and thus scales with the fourth power of the pump fluence (se section SI 2, Supporting Information). The data set for a different g-NQD on a silver film (Figure S3, Supporting Information) further shows that the degree of photon bunching decreases asymptotically toward unity when the pump fluence increases. This is expected because the probability of populating both TXs and BXs saturates toward unity at very high pump powers. While we can readily acquire $g^{(2)}_{MX}$ using relatively low pump power and observe strong photon bunching and inverse pump fluence scaling of the degree of photon bunching in $g^{(2)}_{MX}$ in all g-NQDs on silver films, we need to increase the pump fluence by more than 1 order of magnitude to get a detectable $g^{(2)}_{MX}$ in the case of reference g-NQDs, and the $g^{(2)}_{MX}$ shows no photon bunching (i.e., R = 1). This provides clear evidence that coupling of our g-NQDs to the silver film contributes a very strong enhancement to the emission of MXs.

To further understand the nature of the enhancement of MX emission, we conduct a systematic analysis on the pump-dependent evolution of the PL spectra of reference g-NQDs and g-NQDs on silver films. As the g-NQD−MN interaction can enhance light absorption together with the emission process, the enhancement of absorption alone can lead to an appearance of a stronger MX band when the PL spectra of g-NQDs on silver films and reference g-NQDs are compared at the same pump fluence. To resolve this issue, we first analyzed the pump-dependent saturation of SX emission and determined the enhancement for the absorption. Our approach was based on the fact that the PL of the SX is given by $I_{SX} = (1 - e^{-\langle N \rangle})$, where $\langle N \rangle$ is the average number of excitons created in a NQD at a given pump fluence.[16] For all of the NQDs with the same absorption cross section, the plot of their PL intensities that are normalized to 1 at the saturation level should collapse onto this curve of I_{SX} (black curve of Figure 2a). On the other hand, the curve should shift toward lower $\langle N \rangle$ values, as indicated by the dashed curve and the arrow in Figure 2a, when the absorption of a NQD is enhanced by a certain factor (e.g., 10).

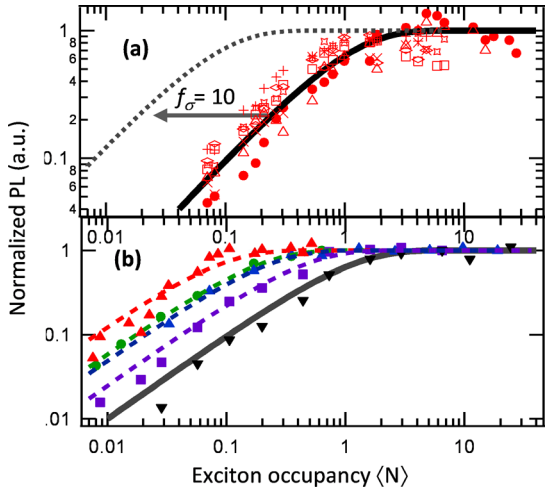

Figure 2. (a) Data points: Normalized PL intensity of SX peaks of five different referenced g-NQDs plotted as a function of average exciton occupancy $\langle N \rangle$. The pump-dependent spectra of one of the g-NQDs (plotted as red solid circles) are displayed as an example in Figure 3, column A. Black solid line: Theoretical saturation curve of SX. A factor of 10 enhancement in absorption should lead to a left shift of the theoretical saturation curve, as indicated by the dotted line and the arrow. (b) Normalized PL intensity of the SX peak of five different g-NQDs on silver film plotted as the function of average exciton occupancy $\langle N \rangle$. Shifts of the plot toward lower $\langle N \rangle$ values provide clear evidence of enhancements in absorption. Black (solid), purple, blue, green, and red (dashes) lines represent the theoretical saturation curves with f_σ of 1, 2.5, 5.2, 6, and 10, respectively.

In Figure 2a, we plotted the normalized PL of the SX emissions of seven reference g-NQDs as a function of $\langle N \rangle$, which is calculated from the pump fluence and absorption cross section (1.23×10^{-13}cm^{-2}) estimated from the average volume of NQDs.[35] As expected, all of the data points of the plot fall very close to the saturation curve. On the other hand, the normalized SX PL versus $\langle N \rangle$ plots of most of the g-NQDs on silver films (Figure 2b) are shifted toward the left, clearly indicating a significant increase in the effective value of $\langle N \rangle$ ($\langle N \rangle_{eff}$), which can be defined as $\langle N \rangle_{eff} = \langle N \rangle \cdot f_\sigma$, where f_σ is the absorption enhancement factor. By shifting the theoretical saturation curves to give a best fit (see dashed lines with the same color), we determine f_σ for the g-NQDs shown in Figure 2b to be 1.0, 2.5, 5.2, 6.0, and 10, respectively. Our analysis on 15 g-NQDs on silver films revealed that f_σ values widely vary within the range of 1−10 and show no correlated variation trend with τ_{SX} (Figure S4, Supporting Information).

Using f_σ values, we calculated $\langle N \rangle_{eff}$ of g-NQD on a silver film and compare the spectra taken at similar $\langle N \rangle$ (in the case of reference g-NQDs) and $\langle N \rangle_{eff}$ values to investigate the effect of plasmons on MX emission. In Figure 3, we display pump-dependent PL spectra of the reference g-NQD (Figure 3a), and four different g-NQDs (Figure 3b−e) on the silver film as examples. These g-NQDs have τ_{SX}'s of 8.4, 2.8, 3.6, 1.3, and 0.83 ns, Q_{BX}/Q_{SX} ratios of 0.4, 0.5, 0.6, 0.4 and 0.8, (Figure S5, Supporting Information), and f_σ's of 5.2, 2.5, 1.0, and 10, respectively. As represented by the reference g-NQD of Figure 3a, the SX peak dominates the PL spectra at all pump fluences in all reference g-NQDs. The BX and higher-order MX bands emerge only at very high pump fluences and get progressively weaker with increasing order m. The spectra for g-NQD on a silver film, on the other hand, clearly revealed that the emission of MXs is strongly enhanced compared to those of reference g-

dx.doi.org/10.1021/jz400479t | J. Phys. Chem. Lett. 2013, 4, 1465−1470

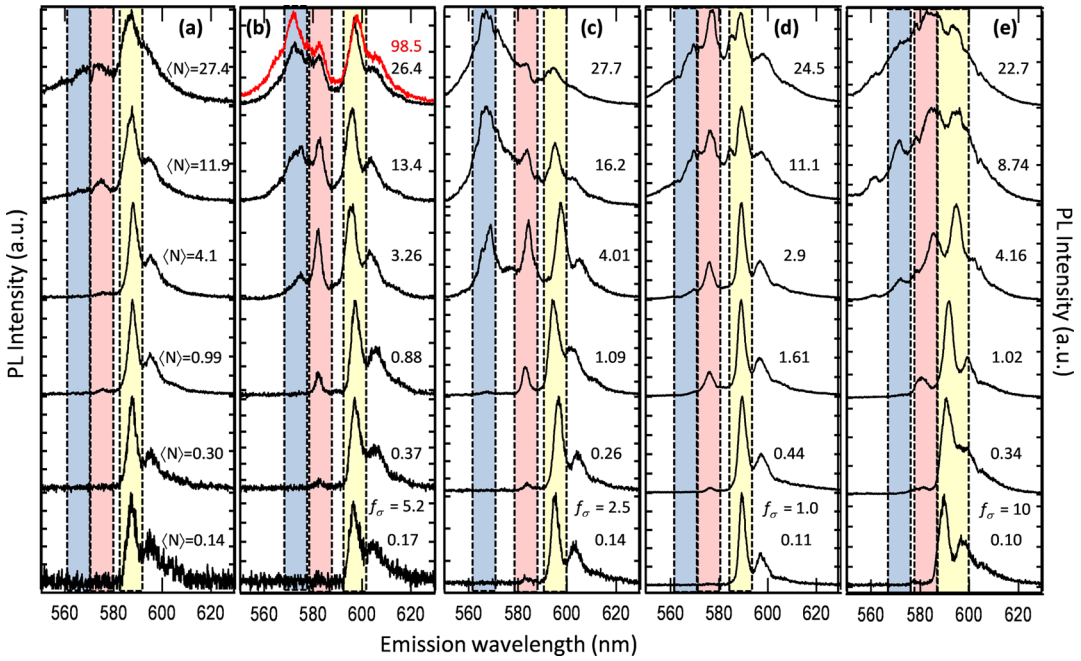

Figure 3. Low-temperature PL spectra of (a) a reference g-NQD as a function of $\langle N \rangle$ and (b–e) four different g-NQDs on silver film as a function of $\langle N \rangle_{eff}$. Spectra of similar $\langle N \rangle$ or $\langle N \rangle_{eff}$ are organized in the same row.

NQDs at the same exciton occupancy. The data even show that the PL peaks of higher-order MXs in case of dots B and C can become stronger than those of BXs and SXs at the highest $\langle N \rangle_{eff}$'s.

Figure 4 shows PL peak intensities of SXs, BXs, and higher-order MXs as a function of $\langle N \rangle$ or $\langle N \rangle_{eff}$. The PL of BX and

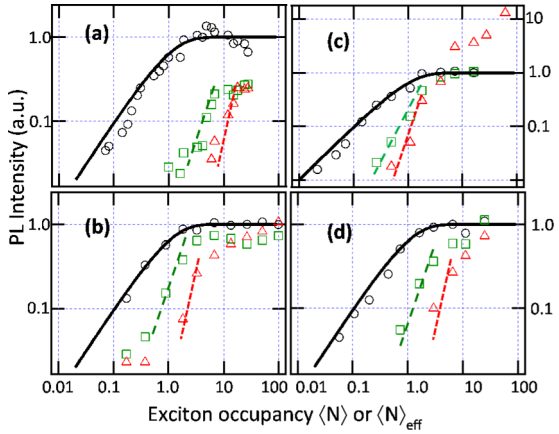

Figure 4. (a–d) Normalized PL intensities of SX (circles), BX (squares), and higher-order MX (triangles) bands of the g-NQDs of Figure 3a–d plotted as a function of exciton occupancy in the same order as Figure 3. Black solid line: Theoretical SX saturation curve. Green dashed and red dotted lines show $\langle N \rangle^2$ and $\langle N \rangle^3$ scaling, respectively.

MX is normalized using the same factor as that for SX. In this case, it can be shown that the normalized PL of BX should rise quadratically with $\langle N \rangle$ and saturates to the R value when $\langle N \rangle$ becomes $\gg 1$ (see SI 7, Supporting Information). For the reference g-NQD of Figure 3a, the graph for the normalized PL of the BX peak (Figure 4a squares) indeed shows that the data points rise quadratically with $\langle N \rangle$ (green dashed line), as expected, and saturate to a maximum value that is close to ~30% of the saturation level of the SX emission (black solid line). A slight discrepancy between the measured R value of 0.4 and saturation level of 0.3 could result from inaccuracies in the estimation of the BX intensity. The plot for the normalized PL of the MX peak (triangles of Figure 4a) shows cubic scaling with $\langle N \rangle$ (red dotted line), which is consistent with the rise of the triexciton state and also shows saturation.

Despite having a very similar R value of 0.5, the BX peak of g-NQD shown in Figure 3b becomes detectable at nearly 1 order of magnitude lower $\langle N \rangle_{eff}$ values, and its normalized PL intensity saturates to a peak value of 0.6, which is slightly higher than the measured R value of 0.5 (Figure 4b, green squares). The higher-order MX band also becomes visible at much lower pump fluences, and its normalized PL exhibits a cubic scaling with $\langle N \rangle_{eff}$ (Figure 4b red triangles). However, instead of saturating, it becomes stronger with the increase of $\langle N \rangle_{eff}$ and finally dominates the spectrum. A similar trend can be observed more clearly for g-NQD of Figure 3c, which is characterized with an R value of 0.6. In this case, BX emission can reach the same level as that of the SX (Figure 4c). Although the MX peaks emerge as an isolated, relatively narrow spectral feature at intermediate pump fluences, it becomes a broad band composed of multiple peaks at high $\langle N \rangle_{eff}$. This suggests that strongly enhanced emission of higher-order MXs (e.g., m = 4 and 5 exciton states) may be responsible for the continuous rise of the MX band. We observed this type of strong enhancement in ~60% of over 30 different g-NQDs on silver films that we investigated.

In the case of the g-NQDs of Figure 3d and e, while the BX and higher-order MX peaks emerge very rapidly at low $\langle N \rangle_{eff}$, as in the previous cases, higher-order MX emission remains weaker compare to that of BX and SX emissions even at the highest $\langle N \rangle_{eff}$. The normalized PL intensities of BX and MX in this case rise only to that of SX and show quadratic and cubic scaling, respectively (Figure 4d). We observe this type of moderate enhancement of MX emission in ~40% of g-NQDs on silver films. This variation among different g-NQDs can be

dx.doi.org/10.1021/jz400479t | J. Phys. Chem. Lett. 2013, 4, 1465–1470

explained as the consequence of the complex electronic structure of MXs. Recent theoretical studies revealed that even a BX of a NQD can have three energetically distinct fine structure states.[36] This multiplicity of fine structure states could only increase further for higher-order MXs. MXs therefore are expected to have multiple, energetically distinct transitions with dipoles varying not only in strengths but also in their orientations. When NQDs with random orientations are coupled to a plasmonic field, we can expect the plasmonic enhancement of MXs to widely vary from one NQD to another depending on how a particular MX transition dipole aligns with the direction of the plasmonic field.

These findings allow us to conclude that the MX emissions in MN−g-NQD coupled systems were enhanced not only through the creation of more excitons via enhancement of absorption but also through the direct modification on the competition between the radiative and nonradiative recombination processes of MXs. More surprisingly, the observation that g-NQDs with relatively low f_σ (e.g., g-NQD C with f_σ =2.5) exhibits much stronger MX emission compared to the case of g-NQD with higher f_σ (e.g., g-NQD E with f_σ =10) points to the conclusion that there may not be any correlation between enhancement of absorption and emission processes. Furthermore, contribution of higher-order MX emission (m = 4 and 5) in the continuous rise of the MX band at the highest $\langle N\rangle_{\mathrm{eff}}$'s provides some indications that the enhancement to the emission process seems to be getting stronger with the increase of multiexciton order. However, due to the overlap of MX emission peaks of different exciton multiplicity and very fast (i.e., faster than instrument response) decay of MX emission, we were not able to quantitatively determine the enhancement factors for different MX emissions. The exact mechanism responsible for this enhancement is also not well understood at this moment. In addition to the enhancement of radiative processes of MXs, the plasmonic field can also modify the nonradiative Auger process. Whether this modification would be the same for MXs of different orders or vary widely from one MX state to another remains unexplored. Furthermore, while the AR dominates the nonradiative recombination of MXs in the case of reference g-NQDs, PL quenching due to the transfer of photogenerated carriers (charge transfer) or the transfer of optical excitation energy (Förster energy transfer) could also become a competing nonradiative process for MXs in the case of g-NQDs deposited on a silver film. A theoretical investigation is necessary to understand how the interplay of these quenching processes, AR, and enhancement of radiative processes give rise to the enhancement of the MX emission. Such detailed understanding could reveal the path toward utilizing g-NQD−MN coupled systems in lasers and photon pair source applications.

■ ASSOCIATED CONTENT

Supporting Information

SI 1. Preparation of silver nanoflakes films; SI 2. the degree of photon bunching in $g^{(2)}$ functions; SI 3. distributions of τ_{SX} and R's of $g^{(2)}$ functions; SI 4. more representative data for individual g-NQDs on Ag films; SI 5. distribution of τ_{SX}'s and f_σ's; SI 6. PL decay curves and $g^{(2)}$ functions; and SI 7. single-exciton and biexciton PL intensities. This material is available free of charge via the Internet at http://pubs.acs.org.

■ AUTHOR INFORMATION

Corresponding Author

*E-mail: htoon@lanl.gov.

Present Address

[§]Young-Shin Park, Center for High Technology Materials, University of New Mexico, Albuquerque, New Mexico 87131, United States.

Notes

The authors declare no competing financial interest.

■ ACKNOWLEDGMENTS

This work was conducted, in part, at the Center for Integrated Nanotechnologies (CINT), a U.S. Department of Energy, Office of Basic Energy Sciences (OBES) user facility. Y.-S.P. is supported by CINT. Y.G. acknowledges Los Alamos National Laboratory Directed Research and Development Funds. H.H. and J.A.H. acknowledge a Single-Investigator Small-Group Research Award (2009LANL1096), OBES, OS, U.S. DOE.

■ REFERENCES

(1) Fafard, S.; Hinzer, K.; Raymond, S.; Dion, M.; McCaffrey, J.; Feng, Y.; Charbonneau, S. Red-Emitting Semiconductor Quantum Dot Lasers. *Science* **1996**, *274*, 1350−1353.

(2) Fafard, S.; Wasilewski, Z. R.; Allen, C. N.; Picard, D.; Piva, P. G.; McCaffrey, J. P. Self-Assembled Quantum Dots: Five Years Later. *Superlattices Microstruct.* **1999**, *25*, 87−96.

(3) Dousse, A.; Suffczynski, J.; Beveratos, A.; Krebs, O.; Lemaitre, A.; Sagnes, I.; Bloch, J.; Voisin, P.; Senellart, P. Ultrabright Source of Entangled Photon Pairs. *Nature* **2010**, *466*, 217−220.

(4) Stevenson, R. M.; Young, R. J.; Atkinson, P.; Cooper, K.; Ritchie, D. A.; Shields, A. J. A Semiconductor Source of Triggered Entangled Photon Pairs. *Nature* **2006**, *439*, 179−182.

(5) Shields, A. J. Semiconductor Quantum Light Sources. *Nat. Photonics* **2007**, *1*, 215−223.

(6) Klimov, V. I.; Mikhailovsky, A. A.; McBranch, D. W.; Leatherdale, C. A.; Bawendi, M. G. Quantization of Multiparticle Auger Rates in Semiconductor Quantum Dots. *Science* **2000**, *287*, 1011−1013.

(7) Htoon, H.; Malko, A. V.; Bussian, D.; Vela, J.; Chen, Y.; Hollingsworth, J. A.; Klimov, V. I. Highly Emissive Multiexcitons in Steady-State Photoluminescence of Individual "Giant" CdSe/CdS Core/Shell Nanocrystals. *Nano Lett.* **2010**, *10*, 2401−2407.

(8) Osovsky, R.; Cheskis, D.; Kloper, V.; Sashchiuk, A.; Kroner, M.; Lifshitz, E. Continuous-Wave Pumping of Multiexciton Bands in the Photoluminescence Spectrum of a Single CdTe−CdSe Core−Shell Colloidal Quantum Dot. *Phys. Rev. Lett.* **2009**, *102*, 197401.

(9) Louyer, Y.; Biadala, L.; Trebbia, J. B.; Fernee, M. J.; Tamarat, P.; Lounis, B. Efficient Biexciton Emission in Elongated CdSe/ZnS Nanocrystals. *Nano Lett.* **2011**, *11*, 4370−4375.

(10) Wang, X.; Ren, X.; Kahen, K.; Hahn, M. A.; Rajeswaran, M.; Maccagnano-Zacher, S.; Silcox, J.; Cragg, G. E.; Efros, A. L.; Krauss, T. D. Non-Blinking Semiconductor Nanocrystals. *Nature* **2009**, *459*, 686−689.

(11) Chen, Y.; Vela, J.; Htoon, H.; Casson, J. L.; Werder, D. J.; Bussian, D. A.; Klimov, V. I.; Hollingsworth, J. A. "Giant" Multishell CdSe Nanocrystal Quantum Dots with Suppressed Blinking. *J. Am. Chem. Soc.* **2008**, *130*, 5026.

(12) Ghosh, Y.; Mangum, B. D.; Casson, J. L.; Williams, D. J.; Htoon, H.; Hollingsworth, J. A. New Insights into the Complexities of Shell Growth and the Strong Influence of Particle Volume in Nonblinking "Giant" Core/Shell Nanocrystal Quantum Dots. *J. Am. Chem. Soc.* **2012**, *134*, 9634−9643.

(13) Dennis, A. M.; Mangum, B. D.; Piryatinski, A.; Park, Y.-S.; Hannah, D. C.; Casson, J. L.; Williams, D. J.; Schaller, R. D.; Htoon, H.; Hollingsworth, J. A. Suppressed Blinking and Auger Recombination in Near-Infrared Type-II InP/CdS Nanocrystal Quantum Dots. *Nano Lett.* **2012**, *12*, 5545−5551.

(14) Mahler, B.; Spinicelli, P.; Buil, S.; Quelin, X.; Hermier, J.-P.; Dubertret, B. Towards Non-Blinking Colloidal Quantum Dots. *Nat. Mater.* **2008**, *7*, 659−664.
(15) García-Santamaría, F.; Brovelli, S.; Viswanatha, R.; Hollingsworth, J. A.; Htoon, H.; Crooker, S. A.; Klimov, V. I. Breakdown of Volume Scaling in Auger Recombination in CdSe/CdS Heteronanocrystals: The Role of the Core−Shell Interface. *Nano Lett.* **2011**, *11*, 687−693.
(16) Park, Y.-S.; Malko, A. V.; Vela, J.; Chen, Y.; Ghosh, Y.; García-Santamaría, F.; Hollingsworth, J. A.; Klimov, V. I.; Htoon, H. Near-Unity Quantum Yields of Biexciton Emission from CdSe/CdS Nanocrystals Measured Using Single-Particle Spectroscopy. *Phys. Rev. Lett.* **2011**, *106*, 187401.
(17) Klimov, V. I.; McGuire, J. A.; Schaller, R. D.; Rupasov, V. I. Scaling of Multiexciton Lifetimes in Semiconductor Nanocrystals. *Phys. Rev. B* **2008**, *77*, 195324.
(18) Schuller, J. A.; Barnard, E. S.; Cai, W.; Jun, Y. C.; White, J. S.; Brongersma, M. L. Plasmonics for Extreme Light Concentration and Manipulation. *Nat. Mater.* **2010**, *9*, 193−204.
(19) Zurita-Sanchez, J. R.; Novotny, L. Multipolar Interband Absorption in a Semiconductor Quantum Dot. I. Electric Quadrupole Enhancement. *J. Opt. Soc. Am. B* **2002**, *19*, 1355−1362.
(20) Zurita-Sanchez, J. R.; Novotny, L. Multipolar Interband Absorption in a Semiconductor Quantum Dot. II. Magnetic Dipole Enhancement. *J. Opt. Soc. Am. B* **2002**, *19*, 2722−2726.
(21) Shimizu, K. T.; Woo, W. K.; Fisher, B. R.; Eisler, H. J.; Bawendi, M. G. Surface-Enhanced Emission from Single Semiconductor Nanocrystals. *Phys. Rev. Lett.* **2002**, *89*, 117401.
(22) Ratchford, D.; Shafiei, F.; Kim, S.; Gray, S. K.; Li, X. Manipulating Coupling between a Single Semiconductor Quantum Dot and Single Gold Nanoparticle. *Nano Lett.* **2011**, *11*, 1049−1054.
(23) Munechika, K.; Chen, Y. C.; Tillack, A. F.; Kulkarni, A. P.; Jen-La Plante, I.; Munro, A. M.; Ginger, D. S. Quantum Dot/Plasmonic Nanoparticle Metachromophores with Quantum Yields That Vary with Excitation Wavelength. *Nano Lett.* **2011**, *11*, 2725−2730.
(24) Bayer, M.; Gutbrod, T.; Forchel, A.; Kulakovskii, V. D.; Gorbunov, A.; Michel, M.; Steffen, R.; Wang, K. H. Exciton Complexes in $In_xGa_{1-x}As/GaAs$ Quantum Dots. *Phys. Rev. B* **1998**, *58*, 4740−4753.
(25) Bayer, M.; Stern, O.; Hawrylak, P.; Fafard, S.; Forchel, A. Hidden Symmetries in the Energy Levels of Excitonic 'Artificial Atoms'. *Nature* **2000**, *405*, 923−926.
(26) Mack, N. H.; Bailey, J. A.; Doorn, S. K.; Chen, C.-A.; Gau, H.-M.; Xu, P.; Williams, D. J.; Akhadov, E. A.; Wang, H.-L. Mechanistic Study of Silver Nanoparticle Formation on Conducting Polymer Surfaces. *Langmuir* **2011**, *27*, 4979−4985.
(27) Vela, J.; Htoon, H.; Chen, Y.; Park, Y.-S.; Ghosh, Y.; Goodwin, P.; Werner, J. H.; Wells, N. P.; Casson, J. L.; Hollingsworth, J. A. Effect of Shell Thickness and Composition on Blinking Suppression and the Blinking Mechanism in 'Giant' CdSe/CdS Nanocrystal Quantum Dots. *J. Biophotonics* **2010**, *3*, 706−717.
(28) Nair, G.; Zhao, J.; Bawendi, M. G. Biexciton Quantum Yield of Single Semiconductor Nanocrystals from Photon Statistics. *Nano Lett.* **2011**, *11*, 1136−1140.
(29) Park, Y.-S.; Ghosh, Y.; Chen, Y.; Piryatinski, A.; Xu, P.; Mack, N. H.; Wang, H.-L.; Klimov, V. I.; Hollingsworth, J. A.; Htoon, H. Super-Poissonian Statistics of Photon Emission from Single Core/Shell Nanocrystals Coupled to Metal Nanostructures. *Phys. Rev. Lett.* **2013**, *110*, 117401.
(30) Akopian, N.; Lindner, N. H.; Poem, E.; Berlatzky, Y.; Avron, J.; Gershoni, D.; Gerardot, B. D.; Petroff, P. M. Entangled Photon Pairs from Semiconductor Quantum Dots. *Phys. Rev. Lett.* **2006**, *96*, 130501.
(31) Dekel, E.; Regelman, D. V.; Gershoni, D.; Ehrenfreund, E.; Schoenfeld, W. V.; Petroff, P. M. Cascade Evolution and Radiative Recombination of Quantum Dot Multiexcitons Studied by Time-Resolved Spectroscopy. *Phys. Rev. B.* **2000**, *62*, 11038−11045.
(32) Korkusinski, M.; Reimer, M. E.; Williams, R. L.; Hawrylak, P. Engineering Photon Cascades from Multiexciton Complexes in a Self-Assembled Quantum Dot by a Lateral Electric Field. *Phys. Rev. B* **2009**, *79*, 035309.
(33) Santori, C.; Fattal, D.; Pelton, M.; Solomon, G. S.; Yamamoto, Y. Polarization-Correlated Photon Pairs from a Single Quantum Dot. *Phys. Rev. B.* **2002**, *66*, 045308.
(34) Fisher, B.; Caruge, J. M.; Zehnder, D.; Bawendi, M. Room-Temperature Ordered Photon Emission from Multiexciton States in Single CdSe Core−Shell Nanocrystals. *Phys. Rev. Lett.* **2005**, *94*, 087403.
(35) See the Supporting Information of ref 16 for calculation of the absorption cross section.
(36) Rodina, A. V.; Efros, A. L. Band-Edge Biexciton in Nanocrystals of Semiconductors with a Degenerate Valence Band. *Phys. Rev. B* **2010**, *82*, 125324.